^{3}H Dendrimer Nanoparticle Organ/Tumor Distribution

Shraddha S. Nigavekar,[1] Lok Yun Sung,[1] Mikel Llanes,[1] Areej El-Jawahri,[1] Theodore S. Lawrence,[1] Christopher W. Becker,[2] Lajos Balogh[3,5] and Mohamed K. Khan[1,4,5]

Received November 7, 2003; accepted November 18, 2003

Purpose. To determine the *in vivo* biodistribution for differently charged poly(amidoamine) (PAMAM) dendrimers in B16 melanoma and DU145 human prostate cancer mouse tumor model systems.
Methods. Neutral (NSD) and positive surface charged (PSD) generation 5 (d = 5 nm) PAMAM dendrimers were synthesized by using ^{3}H-labeled acetic anhydride and tested *in vivo*. Dendrimer derivatives were injected intravenously, and their biodistribution was determined via liquid scintillation counting of tritium in tissue and excretory samples. Mice were also monitored for acute toxicity.
Results. Both PSD and NSD localized to major organs and tumor. Dendrimers cleared rapidly from blood, with deposition peaking at 1 h for most organs and stabilizing from 24 h to 7 days postinjection. Maximal excretion occurred via urine within 24 h postinjection. Neither dendrimer showed acute toxicity.
Conclusions. Changes in the net surface charge of polycationic PAMAMs modify their biodistribution. PSD deposition into tissues is higher than NSD, although the biodistribution trend is similar. Highest levels were found in lungs, liver, and kidney, followed by those in tumor, heart, pancreas, and spleen, while lowest levels were found in brain. These nanoparticles could have future utility as systemic biomedical delivery devices.

KEY WORDS: biodistribution; melanoma; PAMAM dendrimers; prostate cancer; tritiated nanoparticles.

INTRODUCTION

We report the biodistribution of generation 5 poly(amidoamine) (PAMAM) dendrimer derivatives in a mouse tumor model system. PAMAM dendrimers are commercially available macromolecules that can efficiently be used (1–6) as delivery vehicles for oligonucleotides, antisense oligonucleotides, and as probes for oligonucleotide arrays (6–8). PAMAM dendrimers are being investigated for drug delivery, gene therapy, and imaging systems (4–6,9–15).

The evaluation of drug delivery, including dendrimers carrying a targeting moiety attached to their surface, requires the knowledge of the biodistribution of the same carrier dendrimers minus the specific targeting groups. It is expected that size and charge will change the interaction of dendrimers with the cell membrane, thus influencing the nonspecific uptake of these carrier molecules. Generation 4 PAMAMs do not have the necessary dendritic properties to be an effective drug carrier (1,2) whereas generation 6 and 7 PAMAM materials are still too expensive. Generation 5 PAMAM dendrimers have successfully been used in several medical research areas (1,2,4–6,9,12–14), but the role of their charge distribution has not been studied.

Earlier biodistribution studies of PAMAM dendrimers have been carried out with full generation PAMAM dendrimers that were radiolabeled by partially quaternizing the amine termini using ^{14}C containing methyl iodide (16). Commercial Starburst PAMAM dendrimers are a mixture of macromolecules containing minor imperfections, which reduces the total number of available terminal groups (17). Labeling PAMAM Starbursts with ^{13}C iodomethane results in a mixture of quaternized and unquaternized dendrimer end groups in which the radiolabeled macromolecules carry permanent positive charges whereas the charge of unlabeled species depends on the pH. In this mixture, the biodistribution of quaternized (i.e., radiolabeled = charged) macromolecules could be different from the biodistribution of unquaternized molecules because the terminal primary amines are not protonated at biologic pH values and thus are not charged (18). If biodistribution depends on the dendrimer charge, this labeling method may lead to data in which the distribution of labeled molecules is different from the overall distribution of the dendrimers.

The starting PAMAM_E5.NH_2 proved to be toxic to the mice (12). We hypothesized that decreasing the surface charge of PAMAM dendrimers toward neutral would reduces *in vivo* toxicity. This can be achieved by acetylation (14). Transformation of the primary amine groups with an anhydride is a very straightforward and quantitative reaction that results in acetamide termini (19). We synthesized a fully acetylated dendrimer, with a neutral surface, and a partially acetylated product, with a partially positive surface charge (both products had differing net positive overall charge due to the partially protonated internal tertiary nitrogen atoms). We examined the biodistribution and the toxicity of 5 nm tritiated PAMAM dendrimer nanoparticles that have different surface charges [neutral surface dendrimer (NSD) and positive surface dendrimer (PSD)] in normal and tumor tissues.

MATERIALS AND METHODS

Synthesis and Characterization of Tritium-Labeled PAMAM Dendrimers

Chemicals (acetic anhydride, pyridine, MeOH, HCl, NaOH) were purchased from Aldrich (Milwaukee, WI, USA). Solvents were HPLC grade. PAMAM_E5.NH_2, ethylenediamine (EDA) core, generation five, amine-terminated poly(amidoamine) (PAMAM) dendrimer was purchased from Dendritech (Midland, MI, USA) in methanol solution and was further purified by dialysis using reconstructed cellulose membranes (Pierce, molecular weight cut-off (MWCO) = 10 kDa (kilodaltons) to remove potential small molecular contamination such as excess solvent, salts, and trailing generations. The materials were lyophilized and ana-

[1] Department of Radiation Oncology, University of Michigan, Ann Arbor, MI 48109.
[2] Michigan Memorial Phoenix Project, University of Michigan, Ann Arbor, MI 48109.
[3] Department of Internal Medicine, Center for Biologic Nanotechnology, University of Michigan, Ann Arbor, MI 48109.
[4] To whom correspondence should be addressed. (e-mail: mokhan@umich.edu)
[5] Contributed equally to this research.

ABBREVIATIONS: NSD, neutral surface dendrimer; PAMAM, poly(amidoamine); PSD, positive surface dendrimer.

0724-8741/04/0300-0476/0 © 2004 Plenum Publishing Corporation

lyzed by ^{1}H NMR, ^{13}C NMR, mass spectrometry, high pressure liquid chromatography (HPLC), polyacrylamide gel electrophoresis (PAGE), and capillary electrophoresis (CE) to ensure purity and homogeneity of the final products. Theoretically, a PAMAM_E5.NH_2 molecule has a molecular weight of 28,825 Da and contains 128 primary amine termini. The practical number of terminal amines for the particular PAMAM dendrimer we used was determined by acid-base titration and was found to be n = 110. The molecular weight of the dendrimer was 26,200 Da (as determined by size exclusion chromatography; SEC).

Tritium-labeled acetic anhydride (100 mCi) was purchased from ICN Biomedicals (Irvine, CA, USA) and mixed with a known amount of absolute acetic anhydride before use to approach a precalculated specific activity in the products necessary to carry out precise tritium measurements. Labeling of PAMAM was performed via acetylation at room temperature in absolute dimethylsulfoxide in the presence of 50 molar% excess of absolute pyridine for one day (Fig. 1). The resulting products were purified by dialysis against distilled water using reconstructed cellulose membranes (MWCO = 10 kDa) while monitoring the diminishing tritium activity in the water. Labeled polymer products were filtered on 0.2 μm Teflon filters and stored as aqueous solutions at 4°C in sealed vials. Purity and integrity of acetylated dendrimers were checked by PAGE, which indicated no degradation. Degree of acylation was determined from the complete mass balance of the total tritium involved. The final measured activity and degree of average substitution for dendrimers PAMAM_E5.$(NHCOCH_3)_{110}$ (or NSD) was 10.27 mCi/g and for PAMAM_E5.$(NH_2)_{44}$ $(NHCOCH_3)_{66}$ (or PSD) was 17.01 mCi/g. Residual free mobile tritium was <0.3% of the total activity at the time of the biodistribution experiment. Tritiated dendrimers were repeatedly purified by dialysis on a 10 kDa MWCO membrane after 11 months. Exchange of tritium with water protons during storage resulted in a 10% decrease in activity in this period of time.

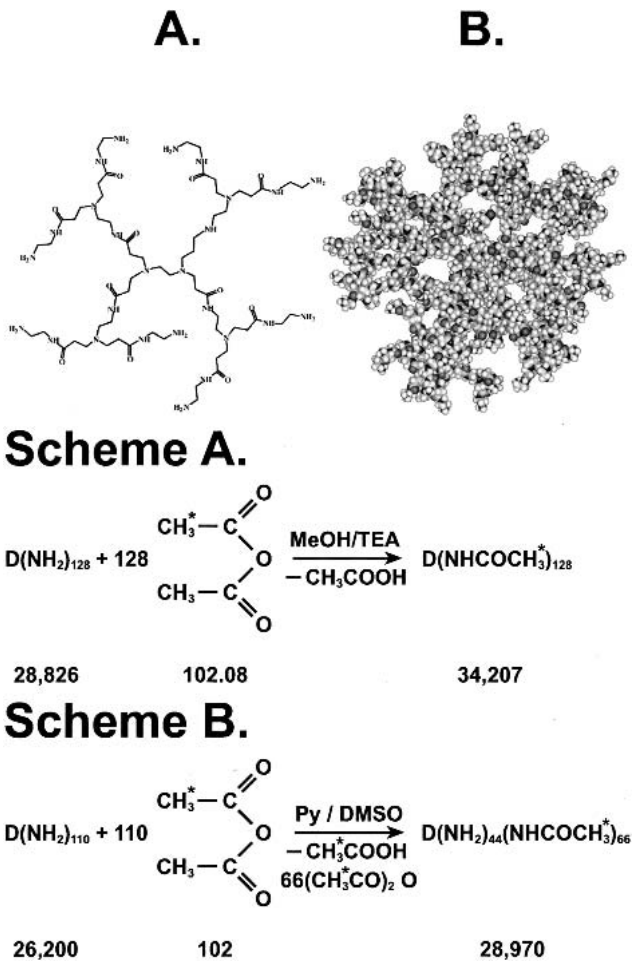

Fig. 1. Structure of poly(amidoamine) dendrimers. (A) Chemical structure of generation 1, ethylenediamine core, amine-terminated PAMAM. (B) Computer model of a generation five macromolecule (courtesy of Inhan Lee, University of Michigan). Schemes of acetylation of PAMAM dendrimers: Scheme A, Scheme of full acetylation based on theoretical numbers. Scheme B, Scheme of partial acetylation based on experimentally determined values. The asterisks denote tritiated hydrogen atoms.

Instrumentation

Analysis of PAMAM dendrimers by PAGE was performed on a Micrograd vertical electrophoresis system with a commercial power supply (Model 500/200; BioRad, Hercules, CA, USA). Electrophoresis experiments were performed on 10 × 8 cm gels in a vertical electrophoresis unit (Model Protean I; BioRad) using precast 4–20% gradient express gels for PAGE (ISC BioExpress). PAGE separations typically required 50 min at 200 V in Tris-Glycine (TG) buffer (pH = 8.3). Developed gels were stained with 0.025% Coomassie blue R-250 overnight.

The CE instrument was purchased from Agilent Technologies (Waldbronn, Germany) and was equipped with an on-capillary UV diode-array detection system. Unmodified quartz capillaries (100 μm ID × 78.5 cm) were obtained from Polymicro Technologies (Phoenix, AZ, USA) and silanized. Samples were introduced by hydrodynamic injection, separation voltage was 20 kV, and the capillary temperature was 40°C for all the separations.

Potentiometric titration was carried out manually, using an Orion Model 230A pH meter (Thermo Electron Corp., Woburn, MA, USA) and an Orion Sure-Flow micropH electrode at room temperature. Approximately 50 mg of PAMAM dendrimer was dissolved in 10 ml of DI water and titrated in 0.1 ml increments with 0.1 N HCl. A 0.1 N NaOH solution was used for back-titration. The number of primary amines was determined from the evaluation of both titration data.

Animal Handling and Tumor Cell Line

Animal work was conducted in the animal facility at University of Michigan Medical Center in accordance with federal, local and institutional guidelines. Experiments adhered to the 'Guide for the Care and Use of Laboratory Animals' (NIH Publication No. 85-23, revised 1985).

Six- to 10-week-old male C57BL/6J mice or 30-week-old male athymic nude (nu/nu) mice were used (Jackson Labs, Bar Harbor, ME, USA). They were caged in a specific pathogen-free barrier facility as groups of five or less and fed *ad libitum* with Laboratory Autoclavable Rodent Diet 5010 (PMI Nutrition International, St. Louis, MO, USA). For excretion studies, five animals were housed in metabolic rodent

cages (Nalgene, Rochester, NY, USA). Anesthesia was via isoflurane inhalation (Abbott Laboratories, North Chicago, IL, USA) prior to surgical procedures. A restrainer (Braintree Scientific Inc., Braintree, MA, USA) was used for tail-vein injections. Euthanasia was with carbon dioxide.

The isogenic B16F10 melanoma cell line was maintained by serial passage within C57BL/6J mice as described previously, with 26 gauge as the smallest needle (20). For biodistribution studies, the B16F10 tumor cells (freshly isolated from carrier mice) were injected subcutaneously into the dorsal surface of 8- to 10-week-old C57BL/6J mice (30 g) and grown until the tumors reached a size of greater than 500 mm^3.

The DU145 human prostate carcinoma cells were grown in culture, and 1.5×10^6 cells were injected subcutaneously into one flank of each athymic nude (nu/nu) mouse (25 g). These slower growing tumors were grown to $\geq$500 mm^3.

Biodistribution Studies and Dendrimer Quantification

When tumors were >500 mm^3, B16 melanoma-bearing mice were injected via tail vein with 500 μl (8.8 μg of PSD and 17.5 μg of NSD) of nanoparticle solution in PBS (Dulbecco's phosphate buffered saline, Sigma-Aldrich, St. Louis, MO, USA). At 5 min, 1 h, and 1, 4, and 7 days postinjection, mice were euthanized and the organs (lung, heart, liver, kidney, spleen, pancreas, tumor, and brain) were dissected and weighed. At all time points, blood samples were collected via cardiac puncture. Typically, each sample of tissues collected ranged between 50 mg to 200 mg. Three to eight mice per nanoparticle per time point were studied. Athymic nude (nu/nu) mice bearing DU145 flank tumors that were at least 500 mm^3 were intravenously injected with PSD, and tissues were harvested at 5 min, 1 h, and 1, 4, and 7 days after injection.

Using metabolic cages, urine and feces were collected at 2, 8, and 24 h postinjection and then once every day for up to 7 days after injection of either dendrimer. Some feces pellets did not roll into the collection tube and absorbed urine (reported as mixed excreta).

To ensure accurate measurement of the low energy beta radiation emitted by tritium, all harvested samples were completely dissolved. One milliliter of "Solvable" solution (Packard, Downers Grove, IL, USA) was added per sample, and the samples were shaken at 50–55°C overnight. They were subsequently decolorized with 200–300 μl of 30% hydrogen peroxide (Sigma-Aldrich). The amount of tritium per sample was determined via liquid scintillation counting using 10 ml Hionic fluor (Packard Bioscience, Downers Grove, IL, USA) per sample. The counts per minute obtained per sample were

Table I. Intraorgan Biodistribution of PAMAM_E5.$(NH_2)_{44}$ $(NHCOCH_3)_{66}$ Positive Surface Dendrimer (PSD) in Liver

Mouse number	1 h		1 Day		4 Day		7 Day	
	1	2	1	2	1	2	1	2
Mean	0.107	0.077	0.078	0.068	0.066	0.053	0.092	0.070
SD	0.013	0.006	0.003	0.002	0.003	0.002	0.003	0.004

Representative data from two B16 melanoma-bearing mice are shown. Seven independent samples from each mouse's liver were collected. The mean (±SD) microcuries of tritium per gram of tissue recovered are shown. The liver intraorgan distribution was seen to be homogenous.

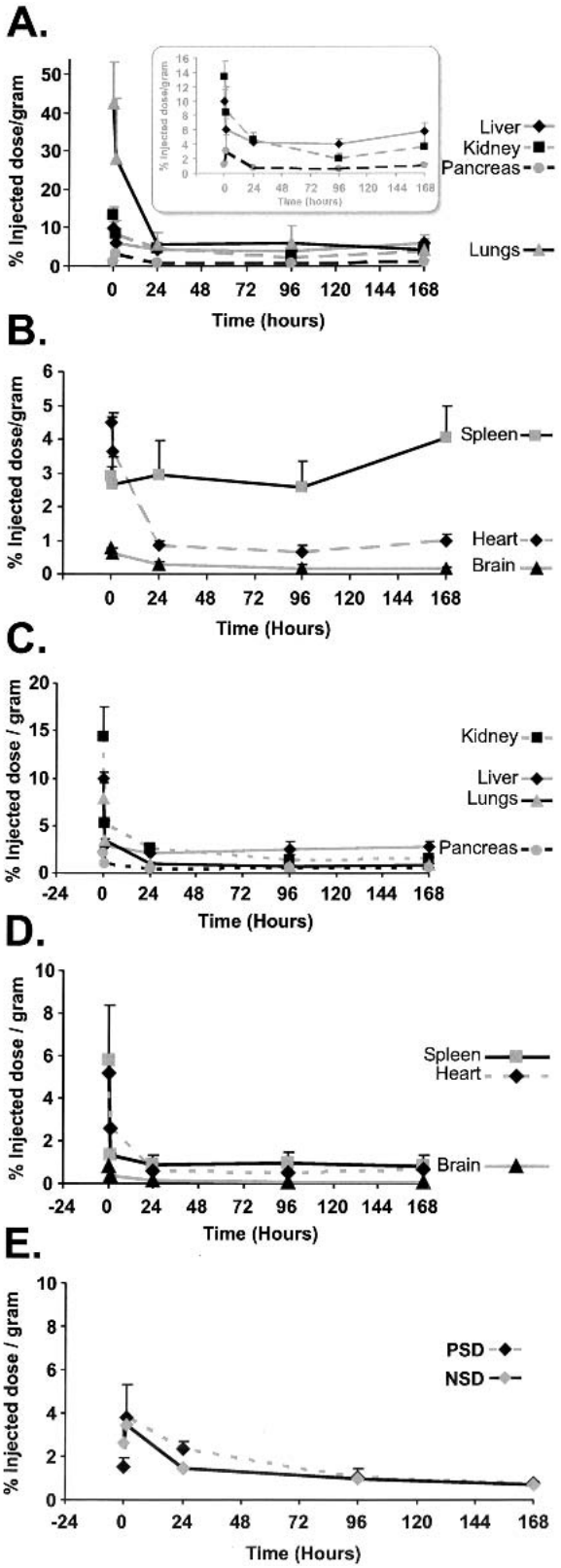

Fig. 2. Biodistribution in C57BL/6J mice (B16 melanoma model), depicted as percent injected dose recovered per gram of organ (% ID/g ± SD) of tritiated dendrimers (n = 4 to 8). (A, B) Positive surface dendrimers (PSD). (C, D) Neutral surface dendrimers (NSD). (E) Tumor uptake for PSD and NSD. (A magnified depiction of PSD distribution in liver, kidney and pancreatic tissues is shown as an inset in A.)

corrected for efficiency of counting and used to derive the number of disintegrations per minute and thus radioactivity (microcuries) per sample. The radioactivity per milligram (μCi/mg) recovered from tissues was normalized to the amount of tritium injected per respective mouse (i.e., the injected dose). The results were then expressed as a percentage of the injected dose per gram of tissue (% ID/g). Thus, the resultant organ and tumor biodistribution data are directly comparable between mice and different dendrimer nanoparticles.

RESULTS

Synthesis of Tritium-Labeled Dendrimers

We successfully synthesized and characterized tritiated PAMAM dendrimer based organic nanoparticles with different surface charges (positive and neutral). The dendrimers were modified using ^{3}H labeled acetic anhydride in which the tritium is covalently bound in the methyl groups thus providing stable labels. Tritium facilitated manipulations during *in vivo* experiments. Labels are on the neutral acetamide termini and therefore do not change the charge-dependent response, while reflecting the true dendrimer distribution. The varying degree of acylation may lead to varying levels of tritium activity, but this complication can be circumvented by comparing the measured values to the total injected dose. Regulation of surface charge and labeling was achieved via acetylation by partially or fully reacting terminal primary amine groups of the PAMAM molecules. This synthetic step served two purposes: 1) toxicity caused by the polyamine character (terminal primary amine groups of PAMAM are positively charged at biologic pH values) was eliminated, and 2) stable tritium labels for the nanoparticles were formed. Radioactive labeling of dendrimers by ^{3}H-containing acetic anhydride allowed proper and accurate quantification of the PAMAM derivatives for the true *in vivo* biodistribution as a function of time, because the labels were introduced as termini that did not carry a charge. Partial acetylation of the terminal amine groups produced polycationic dendrimers with decreased but adjustable surface charge, and increasing of the degree of acetylation decreased the surface positive charges.

Intraorgan Distribution and Accuracy of Injection

In order to determine if the vascular delivery of dendrimers could achieve homogenous intraorgan distribution, the tritium in seven samples (obtained from multiple lobes of the liver) was measured. Both PAMAM dendrimers were distributed throughout the liver with very low standard deviation between liver samples at all time points tested (Table I). Homogenous dendrimer uptake within the liver confirmed that a uniform distribution within vascular organs occurred after intravenous administration of dendrimers. Also, comparable dendrimer levels in the livers of different mice showed the reproducibility and accuracy of systemic delivery via tail vein injections.

Organ and Tumor Distribution of Positive and Neutral Surface Dendrimers

Tritiated PSDs and NSDs showed no preferred distribution into any tissue tested. Both nanoparticles localized to all major organs tested, as well as to tumor tissue, and were recoverable within 5 min postinjection. For most tissues, following an initial rapid clearance during the first day postinjection, the nanoparticles were maintained at a relatively stable level with a very slow decline over time (Fig. 2). Within the first hour postinjection, both nanoparticles exhibited the highest uptake in the lungs, kidney, and liver (PSD, 27.9–6.08% ID/g; NSD, 5.3–2.86% ID/g). Levels in tumor, heart, spleen, and pancreas followed this (PSD, 3.26–2.64% ID/g; NSD, 3.44–0.92% ID/g), while the least amount of dendrimers was deposited into brain tissue (PSD, 0.6% ID/g; NSD, 0.39% ID/g).

Both dendrimers cleared rapidly from blood, with 5 min (20.6, 21.6), 1 h (14.3, 9.9), 1 day (1.7, 0.9), 4 days (0.3, 0.1), 7 days (0.2, 0.1) %ID/g levels for (PSD, NSD), respectively.

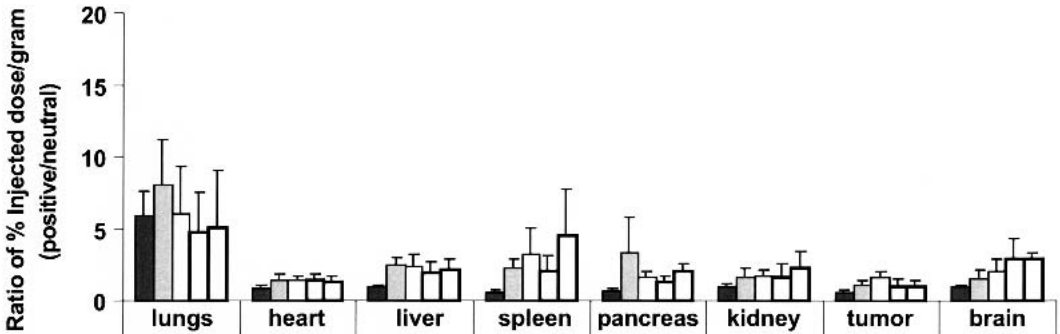

	lungs	heart	liver	spleen	pancreas	kidney	tumor	brain
5 min	5.88	0.86	0.92	0.50	0.61	0.97	0.58	0.96
1	8.04	1.40	2.46	2.25	3.37	1.59	1.06	1.53
1 day	6.05	1.43	2.40	3.21	1.61	1.73	1.61	2.08
4 days	4.70	1.38	1.93	2.09	1.30	1.59	0.94	2.86
7 day	5.07	1.34	2.14	4.53	2.04	2.25	0.99	2.85

Tissues

Fig. 3. Ratio of the percent injected dose per gram of organ (% ID/g) of positive surface dendrimer (PSD) relative to that of the neutral surface dendrimer (NSD) in tissues of C57BL/6J mice (B16 melanoma model). The bars show mean ratios and error bars show total standard deviation.

Most organs showed maximum uptake within 5 min, except tumor and pancreas (maxima at 1 h). Deposition of positive surface dendrimers are higher than neutral surface dendrimers within 1 h postinjection in all organs and tissues analyzed, including tumor tissue (Fig. 3).

The dendrimers were excreted via both urine and feces (Fig. 4). A total of 48.3% of NSD and 29.6% of PSD were excreted via urine over 7 days. Within the first 2 h, urinary NSD excretion was more than 3-fold that of PSD, but at later sampling points the daily excretion of both dendrimers was equivalent. Dendrimers were excreted via feces to a much lesser extent, with a total of 5.41% of NSD and 2.96% of PSD recovered over 7 days (Fig. 4). Thus, the dendrimers were excreted mainly via urine with a significant amount of urinary excretion occurring within 24 h postinjection.

Because tumor-bearing mice would die due to their tumor-burden, long-term biodistribution studies of NSD and PSD were done with normal (non-tumor-bearing) mice. Five mice were injected with either NSD or PSD, and organs were harvested 12 weeks after dendrimer injection. The dendrimers were detectable in all organs tested (Table II). This demonstrated that the nanoparticles could distribute to all organs tested and remain there at relatively stable levels for at least 12 weeks. The mice appeared healthy at that time as well.

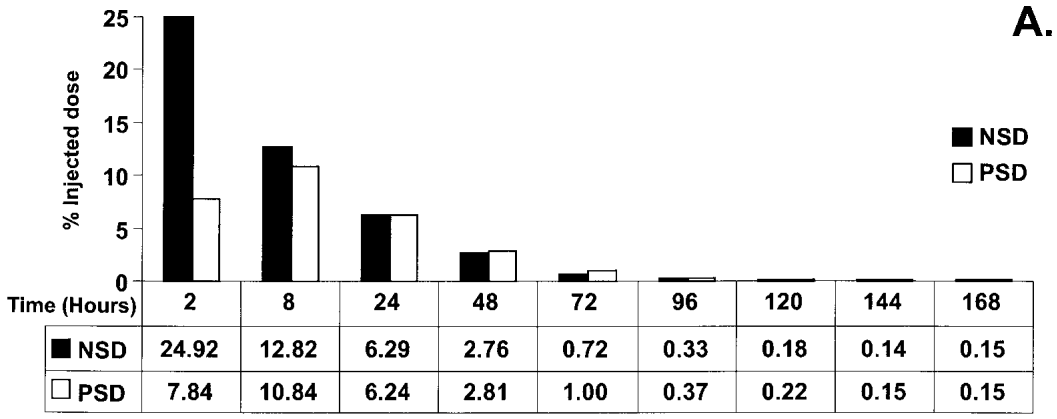

Time (Hours)	2	8	24	48	72	96	120	144	168
NSD	24.92	12.82	6.29	2.76	0.72	0.33	0.18	0.14	0.15
PSD	7.84	10.84	6.24	2.81	1.00	0.37	0.22	0.15	0.15

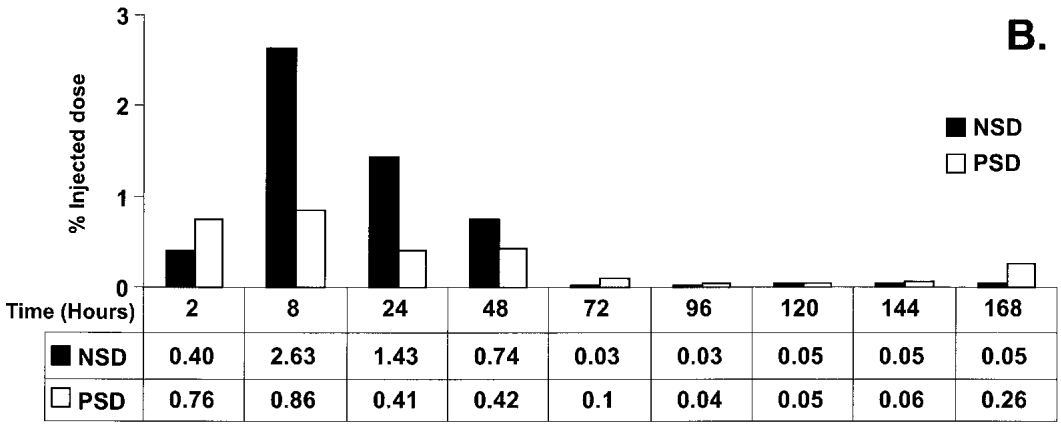

Time (Hours)	2	8	24	48	72	96	120	144	168
NSD	0.40	2.63	1.43	0.74	0.03	0.03	0.05	0.05	0.05
PSD	0.76	0.86	0.41	0.42	0.1	0.04	0.05	0.06	0.26

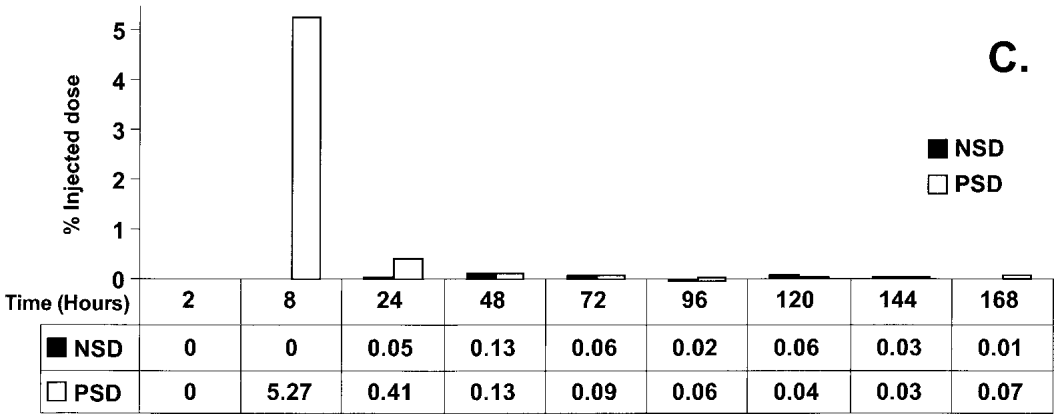

Time (Hours)	2	8	24	48	72	96	120	144	168
NSD	0	0	0.05	0.13	0.06	0.02	0.06	0.03	0.01
PSD	0	5.27	0.41	0.13	0.09	0.06	0.04	0.03	0.07

Fig. 4. Excretion of positive surface dendrimers (PSD) and neutral surface dendrimers (NSD) via urine, feces, and mixed excreta (A, B, and C respectively) at time points indicated. Mixed excreta comprise urine and fecal materials that were inseparable. The data obtained from B16F10 melanoma mouse model (n = 5) is presented as a percentage of injected dose excreted per mouse.

Table II. Long-Term Biodistribution of Dendrimers

	NSD	PSD
Blood	0.02 ± 0.00	0.09 ± 0.01
Lungs	0.13 ± 0.04	0.17 ± 0.08
Heart	0.17 ± 0.02	0.16 ± 0.07
Liver	0.39 ± 0.12	0.37 ± 0.16
Spleen	0.55 ± 0.21	0.52 ± 0.31
Pancreas	0.20 ± 0.03	0.33 ± 0.17
Kidney	0.38 ± 0.10	1.09 ± 0.29
Brain	0.07 ± 0.01	0.11 ± 0.01

Biodistribution of neutral surface dendrimer [NSD, PAMAM_E5.(NHCOCH3)110] and positive surface dendrimer [PSD, PAMAM_E5.(NH2)44 (NHCOCH3)66] at 12 weeks after intravenous injection is shown. The data are from non-tumor-bearing mice (to be able to obtain a longer time point) and are presented as % injected dose/gram ± standard deviation.

Confirmatory Biodistribution in a Human Prostate Cancer Mouse Xenograft Model System

To verify the biodistribution results from B16 melanoma bearing mice, we used an unrelated tumor model system. DU145 human prostate tumor-bearing mouse xenograft (athymic nu/nu) and non-tumor-bearing athymic nude (nu/nu) mice were injected intravenously with PSD. Organs and tumor tissue were harvested at 1 h, 1- and 4-day time points after injection and analyzed for tritium content (see "Materials and Methods"). The results were expressed as the percentage of the injected dose per gram of tissue (% ID/g). The trends of PSD distribution in DU145 prostate tumor-bearing mice and the non-tumor-bearing mice were similar to those observed in the B16 melanoma bearing mice. The only significant difference between the two tumor models was a faster clearance of the PSD in spleens of the DU145 tumor bearing mice (Fig. 5). This indicated that the dendrimer biodistributions are generally applicable, with only minor mouse tumor model effects.

Biological Safety of Dendrimers

There was no acute *in vivo* toxicity noted from the PSD and NSD dendrimer injections. Five mice were injected with 500 μl each of NSD (17.5 μg) and another five mice with PSD (8.8 μg). These mice along with five uninjected control mice were monitored for 12 weeks, noting their weight, signs of dehydration, weakness, lethargy, change in activity, and any inability to eat or drink. The dendrimer-injected groups of mice showed a steady weight gain for 10 days after which the weights were maintained, similar to the control group of mice. No difference was observed between the control group and the dendrimer injected groups of mice for the toxicity parameters monitored.

DISCUSSION AND CONCLUSIONS

It had previously been reported that PAMAM dendrimer toxicity is dose- and generation-dependent, with *intraperitoneal* injections of generation five or smaller dendrimers appearing to be nontoxic *in vivo* (16,21). Previous studies were conducted with *normal* (non-tumor-bearing) mice, in a few tissues, and over a short time period. It is particularly important to evaluate these novel nanoparticles over a prolonged time period, and with intravenous injection, as this is what will occur with human therapy. Both positive surface and neutral surface acetylated PAMAM dendrimers described in this study were placed at pH 7.4 and systemically administered to the mice. The tritiated nanoparticles were not acutely toxic in tumor bearing mice (≤7 days). In non-tumor-bearing injected mice, there were no deleterious effects from the nanoparticles for up to 12 weeks. The partial or full acetylation of the surface amine groups and physiologic pH adjustment renders the PAMAM_E5 dendrimer nanoparticles physiologically tolerable when injected intravenously.

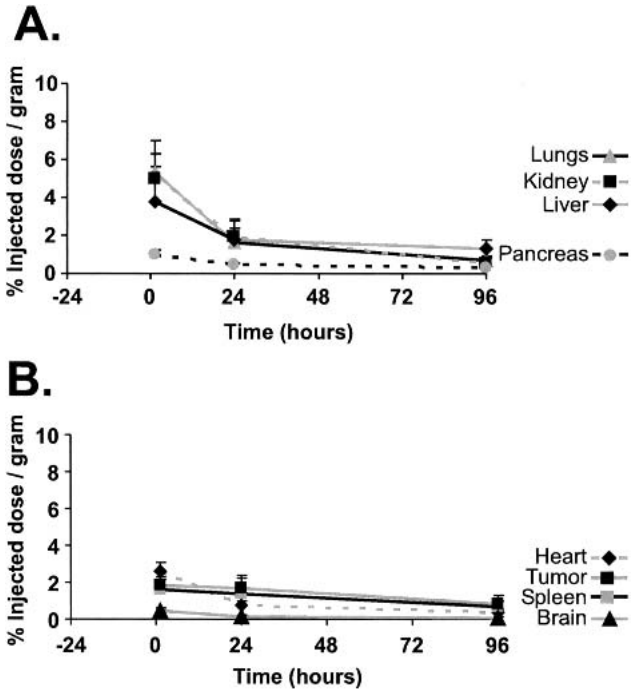

Fig. 5. Biodistribution in athymic nude (nu/nu) mice (DU145 human prostate cancer xenograft model) depicted as percent injected dose recovered per gram of organ (% ID/g ± SD) of PSD. (A, B) tumor-bearing mice (n = 3).

Two types of dendrimer nanoparticles were successfully studied. While both were 5 nm in size, they differed in their surface charge (intentionally modulated to be either neutral or positive). For 5-nm-diameter PAMAM dendrimers, surface charge differences affected the relative deposition of the PAMAM dendrimers, rather than the distribution into organs tested at any given time point, with the PSD showing higher deposition overall.

Neither dendrimer localized selectively to tumor tissue, with distribution to all organs tested. Following an initial rapid clearance during the first day postinjection, nanoparticles were maintained at a relatively stable level in every tissue, with a very slow decline over time. Excretory analyses revealed that the dendrimers were excreted via both urine and feces with maximal excretion occurring via urine within the first 24 h. Urinary NSD amounts excreted exceeded those of PSD by more than 3-fold within 2 h postinjection. This is consistent with more PSD taken up by tissues, and therefore less excreted.

The fact that these nanoparticles distribute into every tissue tested and remain relatively stable over prolonged periods may prove useful in the future for systemic *in vivo* de-

livery of agents (e.g., DNA or drugs) to numerous tissues. Also, because biodistribution in both mouse tumor models was very similar, this mode of systemic dendrimer delivery promises to be generally applicable.

Chemically, it is important to note that practical grade PAMAM dendrimers are not a set of identical, pure, and discrete macromolecules because of their polymer character and minor structural deviations (17). Dendrimers, being spherical polyfunctional macromolecules, are better described by their average molecular mass and molecular mass distribution. Thus, when these macromolecules are reacted to form a derivative, a distribution of substituents will be produced, instead of identical macromolecules with the same degree of substitution (22).

Radiolabeling allows conclusions about the presence of materials by determining the presence of a labeled subset usually by measuring the overall radiation. As labeling of every single molecule would result in enormous level of radioactivity, usually only a subset of molecules carries the radioactive label. This implies that a certain property of the subset represents the whole population. Measuring the average radioactivity in a sample thus represents the distribution of the whole population only if the properties of the measured subset of labeled molecules are identical with the unlabeled ones. Covalent radiolabeling of PAMAM dendrimers with tritium-containing acetic anhydride results in controlled modulation of macromolecular surface charge and fully maintains the chemical characteristics of the nanoparticles reacted with unlabeled reactants.

Following intravenous administration, the PSDs and NSDs were carried via the circulatory system to different parts of the body. We postulate that while the majority of nanoparticles are cleared and excreted, some are deposited into microvasculature of various organ tissues and internalized by the endothelium or cells adjacent to the endothelium. This hypothesis is supported by another study we carried out, in which a 5-nm nonradioactive gold complexed amine surface dendrimer nanoparticle was synthesized and tested. In those studies, the gold nanocomposite solution was directly injected into dorsal B16 melanoma tumors (1) or DU145 prostate tumors (12), and transmission electron microscopy of tumor tissue indicated that the gold nanocomposites rapidly leave the interstitium and are internalized by the cells (1,12).

Tumor growth and successful metastases is dependent on tumor angiogenesis, that is, the formation of new microvessels (23,24). Now that accurate measurement and toxicity tests of the nanoparticles have been demonstrated, in future studies we plan to design nanomolecular devices that localize to tumor cells by exploiting the differences between normal and tumor microvasculature. The tumor microvasculature is leakier then the normal microvasculature (25–29). It has been shown that extravasation of smaller PAMAM dendrimers through the normal microvasculature of hamster muscle is dependent on size and molecular weight (30). Therapies targeted to tumor microvasculature or to the angiogenic process are attractive because they are inherently applicable to all tumors. In conjunction with traditional therapy, anti-angiogenic approaches could help control and/or treat metastases. The biodistribution and biological evaluation studies presented here are an important first step in this process.

This study demonstrates the feasibility of using tritiated PAMAM dendrimers to analyze the effect of nanoparticle charge on *in vivo* biodistribution in mouse tumor model systems and showed the low toxicity of these nanoparticles. We were able to determine that the dendrimers (d = 5 nm) cleared rapidly from the blood, distributed to and remained stable in all organs and tissues tested for at least 7 days in tumor-bearing mice. We also found that PSD deposition into B16 melanoma tumor tissue is almost 1.5 fold as much as that of the NSD within 1 day postinjection. Results were similar in two very different tumor model systems. The ability to build, modulate the surface, and measure these devices accurately over time will have significant implications for the imaging and treatment of variety of local and metastatic tumors.

ACKNOWLEDGMENTS

The U.S. Department of Energy (Award No. FG01-00NE22943) supported this research. S. Nigavekar is supported by a Research Fellowship from the Department of Radiation Oncology, University of Michigan. Donna Livant supplied the DU145 cells. Alla Kwitny and Fatema Mamou assisted during biodistribution studies, Inhan Lee created the dendrimer image, and Steven Kronenberg assisted with graphics.

REFERENCES

1. L. Balogh, A. Bielinska, J. D. Eichman, R. Valluzzi, I. Lee, J. R. Baker, T. S. Lawrence, and M. K. Khan. Dendrimer nanocomposites in medicine. *Chimica Oggi/Chemistry Today* **20**:35–40 (2002).
2. R. Esfand and D. A. Tomalia. Poly(amidoamine) (PAMAM) dendrimers: from biomimicry to drug delivery and biomedical applications. *Drug Discov. Today* **6**:427–436 (2001).
3. J. F. G. A. Jansen, E. M. M. de Brabander-van den Berg, and E. W. Meijer. Encapsulation of guest molecules into a dendritic box. *Science* **266**:1226–1229 (1994).
4. J. D. Eichman, A. U. Bielinska, J. F. Kukowska-Latallo, and J. R. Baker. The use of PAMAM dendrimers in the efficient transfer of genetic material into cells. *Pharmaceutical Science and Technology Today* **3**:232–245 (2000).
5. J. F. Kukowska-Latallo, A. U. Bielinska, J. Johnson, R. Spindler, D. A. Tomalia, and J. R. Baker Jr. Efficient transfer of genetic material into mammalian cells using Starburst polyamidoamine dendrimers. *Proc. Natl. Acad. Sci. U. S. A.* **93**:4897–4902 (1996).
6. A. Bielinska, J. F. Kukowska-Latallo, J. Johnson, D. A. Tomalia, and J. R. Baker Jr. Regulation of in vitro gene expression using antisense oligonucleotides or antisense expression plasmids transfected using starburst PAMAM dendrimers. *Nucleic Acids Res.* **24**:2176–2182 (1996).
7. R. Delong, K. Stephenson, T. Loftus, M. Fisher, S. Alahari, A. Nolting, and R. L. Juliano. Characterization of complexes of oligonucleotides with polyamidoamine starburst dendrimers and effects on intracellular delivery. *J. Pharm. Sci.* **86**:762–764 (1997).
8. H. Yoo, P. Sazani, and R. L. Juliano. PAMAM dendrimers as delivery agents for antisense oligonucleotides. *Pharm. Res.* **16**: 1799–1804 (1999).
9. N. Malik, E. G. Evagorou, and R. Duncan. Dendrimer-platinate: a novel approach to cancer chemotherapy. *Anticancer Drugs* **10**: 767–776 (1999).
10. B. Raduchel, H. Schmitt-Willich, J. Platzek, W. Ebert, T. Frenzel, B. Misselwitz, and H. J. Weinmann. Synthesis and characterization of novel dendrimer-based gadolinium complexes as MRI contrast agents for the vascular system. *Proc. Amer. Chem. Soc. Polym. Mater. Sci. Eng.* **79**:516–517 (1998).
11. H. Kobayashi, N. Sato, S. Kawamoto, T. Saga, A. Hiraga, T. L. Haque, T. Ishimori, J. Konishi, K. Togashi, and M. W. Brechbiel. Comparison of the macromolecular MR contrast agents with ethylenediamine-core versus ammonia-core generation-6 polyamidoamine dendrimer. *Bioconjug. Chem.* **12**:100–107 (2001).
12. L. P. Balogh, S. S. Nigavekar, A. C. Cook, L. Minc, and M. K.

Khan. Development of dendrimer-gold radioactive nanocomposites to treat cancer microvasculature. *PharmaChem* **2**:94–99 (2003).
13. A. Bielinska, J. D. Eichman, I. Lee, J. R. Baker, and L. Balogh. Imaging {Au^0-PAMAM} gold-dendrimer nanocomposites in cells. *J. Nanoparticle Res.* **4**:395–403 (2002).
14. A. Quintana, E. Raczka, L. Piehler, I. Lee, A. Myc, I. Majoros, A. K. Patri, T. Thomas, J. Mule, and J. R. Baker Jr. Design and function of a dendrimer-based therapeutic nanodevice targeted to tumor cells through the folate receptor. *Pharm. Res.* **19**:1310–1316 (2002).
15. S. Shukla, G. Wu, M. Chatterjee, W. Yang, M. Sekido, L. A. Diop, and R. Muller. S. J. J., R. J. Lee, R. F. Barth, and W. Tjarks. Synthesis and biological evaluation of folate receptor-targeted boronated PAMAM dendrimers as potential agents for neutron capture therapy. *Bioconjug. Chem.* **14**:158–167 (2003).
16. J. C. Roberts, M. K. Bhalgat, and R. T. Zera. Preliminary biological evaluation of polyamidoamine (PAMAM) Starburst dendrimers. *J. Biomed. Mater. Res.* **30**:53–65 (1996).
17. J. Peterson, V. Allikmaa, J. Subbi, T. Pehk, and M. Lopp. Structural deviations in poly(amidoamine) dendrimers: a MALDI-TOF MS analysis. *European Polymer J.* **39**:33–42 (2003).
18. D. A. Tomalia, A. M. Naylor, and W. A. Goddard III. Starburst dendrimers: molecular-level control of size, shape, surface chemistry, topology, and flexibility from atoms to macroscopic matter. *Angewandte Chemie International Edition English* **29**:138–175 (1990).
19. I. J. Majoros, B. Keszler, S. Wochler, T. Bull, and J. R. Baker Jr. Acetylation of poly(amidoamine) dendrimers. *Macromolecules* **36**:5526–5529 (2003).
20. M. S. O'Reilly, L. Holmgren, Y. Shing, C. Chen, R. A. Rosenthal, M. Moses, W. S. Lane, Y. Cao, E. H. Sage, and J. Folkman. Angiostatin: a novel angiogenesis inhibitor that mediates the suppression of metastases by a Lewis lung carcinoma. *Cell* **79**:315–328 (1994).
21. D. S. Wilbur, P. M. Pathare, D. K. Hamlin, K. R. Buhler, and R. L. Vessella. Biotin reagents for antibody pretargeting. 3. Synthesis, radioiodination, and evaluation of biotinylated starburst dendrimers. *Bioconjug. Chem.* **9**:813–825 (1998).
22. C. Zhang, S. O'Brien, and L. Balogh. Comparison and Stability of CdSe Nanocrystals Covered with Amphiphilic Poly(Amidoamine) Dendrimers. *J. Phys. Chem. B.* **106**:10316–10321 (2002).
23. J. Folkman. Tumor Angiogenesis. In J. F. Holland, R. C. Bast Jr., D. L. Morton, E. Frie III, D. W. Kufe, and R. R. Weichselbaum (eds.), *Cancer Medicine*, 4th edition, Williams and Wilkens, Baltimore, 1996, pp. 181–204.
24. J. Folkman. Angiogenesis in cancer, vascular, rheumatoid and other disease. *Nat. Med.* **1**:27–31 (1995).
25. H. Hashizume, P. Baluk, S. Morikawa, J. W. McLean, G. Thurston, S. Roberge, R. K. Jain, and D. M. McDonald. Openings between defective endothelial cells explain tumor vessel leakiness. *Am. J. Pathol.* **156**:1363–1380 (2000).
26. L. F. Brown, M. Detmar, K. Claffey, J. A. Nagy, D. Feng, A. M. Dvorak, and H. F. Dvorak. Vascular permeability factor/vascular endothelial growth factor: a multifunctional angiogenic cytokine. *EXS* **79**:233–269 (1997).
27. T. W. Grunt, A. Lametschwandtner, and K. Karrer. The characteristic structural features of the blood vessels of the Lewis lung carcinoma (a light microscopic and scanning electron microscopic study). *Scan. Electron Microsc.* (Pt 2)**2**:575-89. (1986).
28. P. A. Stewart, K. Hayakawa, C. L. Farrell, and R. F. Del Maestro. Quantitative study of microvessel ultrastructure in human peritumoral brain tissue. Evidence for a blood-brain barrier defect. *J. Neurosurg.* **67**:697–705 (1987).
29. J. M. Brown and A. J. Giaccia. The unique physiology of solid tumors: opportunities (and problems) for cancer therapy. *Cancer Res.* **58**:1408–1416 (1998).
30. M. El-Sayed, M. F. Kiani, M. D. Naimark, A. H. Hikal, and H. Ghandehari. Extravasation of poly(amidoamine) (PAMAM) dendrimers across microvascular network endothelium. *Pharm. Res.* **18**:23–28 (2001).